All-electron projector-augmented-wave *GW* approximation: Application to the electronic properties of semiconductors

B. Arnaud and M. Alouani
Institut de Physique et de Chimie des Matériaux de Strasbourg (IPCMS), 23 rue du Loess, 67037 Strasbourg, France
(Received 10 November 1999; revised manuscript received 3 March 2000)

The so-called *GW* approximation (GWA) based on an all-electron full-potential projector-augmented-wave method (PAW) has been implemented. For the screening of the Coulomb interaction *W three* different plasmon-pole model dielectric function models have been tested, and it is shown that the accuracy of the quasiparticle energies is not sensitive to the details of these models. For the decoupling of the valence and core electrons *two* different schemes produced quasiparticle energies that differ on average by less than 0.1 eV for Si. This method has been used to study the quasiparticle band structure of some small, medium, and wide-band-gap semiconductors: Si, GaAs, AlAs, InP, Mg_2Si, diamond, and the insulator LiCl. Special attention was devoted to the convergence of the self-energy with respect to both the **k** points in the Brillouin zone and to the number of reciprocal-space **G** vectors. The most important and surprising result is that although the all-electron GWA improves considerably the local-density approximation electronic structure of semiconductors, it does *not* always provide the correct energy band gaps for small- and medium-band-gap semiconductors as originally inferred from pseudopotential GWA calculations. The discrepancy between the all-electron and pseudopotential quasiparticle band gaps is mainly traced back to differences between the exchange-correlation matrix elements obtained by the two methods.

I. INTRODUCTION

The most successful approach for predicting the quasiparticle (QP) properties of solids from first principles is the so-called *GW* approximation (GWA) of Hedin.[1,2] This remarkable development in the theoretical study of the electronic structure of materials is due to the inclusion of many-body effects in the calculation, principally through the computation of the QP self-energy and the results are an adjustment of the energy splittings obtained within the local-density approximation (LDA).[3–19] Thus this method included efficiently the correlation effects without omitting the subtlety of the chemical bonding unlike the parametrized Hubbard model.

After this initial success the GWA has been extensively used to study physical properties of different types of materials ranging from (1) the bandwidth narrowing in alkali metals and their clusters;[20,21] (2) the surface states of semiconductors, i.e., improving the energy positions of surface states,[22] looking for dimer buckling in Si surfaces;[23] (3) the effects of correlation on the valence off-set between different bulk semiconductors;[24] (4) the character of the band gaps of superlattices and anisotropy of optical matrix elements;[25] (5) the orientational disorder and photoemission spectra of solid C_{60};[15] (6) the electronic properties of bulk Ni and its energy-loss spectra;[14] (7) the electronic properties of atoms using various GWA;[26] (8) the Schottky barrier between a metal and a semiconductor;[27] and (9) the inclusion of excitonic effects in the calculation of the dielectric function of semiconductors.[28–30] All these different studies in a very short time established the GWA as a good ''first-principles'' method for computations of QP properties of *real* materials.

Unfortunately, most of the GWA implementations are based on a plane-wave expansion of the Bloch wave function and on the pseudopotential approach which makes an analysis in terms of chemically relevant orbitals difficult. An additional difficulty with a pure plane wave basis set is that the computational effort for studying systems with localized *d* or *f* electrons is enormous. In this paper, we propose an implementation of the GWA based on an all-electron method using the recently developed all-electron projector-augmented-wave (PAW) method.[31] The knowledge of the all-electron Green's function provided by the PAW method allows us to construct the QP self-energy within the GWA, in which the dynamical screening of the electron-electron interaction arises from a plasmon-pole model dielectric function[9,12,32] for which the parameters are adjusted to the dielectric function calculated in the random-phase approximation[33] (RPA). To check the accuracy of our method we have used three types of plasmon-pole models to describe approximately the screening of the Coulomb interaction, and two different schemes for decoupling the core and valence electrons. This latter point is important because the accuracy of the calculated quasiparticle energies depends on the correct subtraction of the LDA valence-electron exchange-correlation matrix elements from the self-energy.

Our paper is organized as follows: In Sec. II we introduce the projector-augmented-wave method which is used to solve the Kohn-Sham equations and provides the all-electron Green's function and the RPA dielectric function which are the basic ingredients for the computation of the self-energy. We then describe our GWA implementation and discuss in some details the difficult points of this method. In particular, we discuss the difficulty related to the decoupling of the core and valence electrons. The usage of the point-group symmetry to reduce the computational cost of the self-energy and the dielectric function is discussed in the Appendix. In Sec. III we apply our method to compute the electronic structure of two distinct semiconductor groups: some small- and

medium-band-gap semiconductors: Si, GaAs, AlAs, InP, Mg_2Si, and some wide-band-gap semiconductors (insulator): C and (LiCl). We then compare our results with available GWA calculations and experiments.

II. METHOD OF CALCULATION

A. A brief overview of the PAW method

In the density-functional theory implemented in the framework of the LDA,[34] an electronic structure calculation requires the solution of Kohn-Sham type of equations in a self-consistent way. The computation of materials band structure consists of finding the Bloch wave functions $\Psi_{\mathbf{k}n}(\mathbf{r})$, where n and $\mathbf{k}$ denote a band index and a wave vector in the Brillouin zone (BZ), respectively. In the projector-augmented-wave formalism,[31] all calculations are performed using a smooth pseudo-wave-function $\tilde{\Psi}_{\mathbf{k}n}(\mathbf{r})$ which is expressed as a linear combination of plane waves. The passage from the smooth pseudo-wave-function to the all-electron wave function exhibiting the correct nodal behavior in the augmentation regions (spheres centered on each atom) is achieved by defining three atomic types of functions in each augmentation region: (1) the all-electron basis functions $\Phi_i^a(\mathbf{r})$, (2) the pseudo-basis-functions $\tilde{\Phi}_i^a(\mathbf{r})$, and (3) the projector functions $\tilde{p}_i^a(\mathbf{r})$. Here $i=l_i,m_i,n_i$, where l_i and m_i denote the orbital and magnetic quantum numbers, respectively. The index n_i is introduced for a possible choice of more than one function per angular momentum channel (l_i,m_i). These functions are defined so that

$$\tilde{\Phi}_i^a(r)=\Phi_i^a(r) \quad \text{for} \quad r\geqslant r_c^a, \tag{1}$$

where r_c^a are the radii of nonoverlapping spheres centered at each atomic site a. The projector functions vanish for $r \geqslant r_c^a$ and satisfy the orthogonality property:

$$\langle \tilde{p}_i^a|\tilde{\Phi}_j^a\rangle=\delta_{ij}. \tag{2}$$

Using these functions, the all-electron wave function $\Psi_{\mathbf{k}n}(\mathbf{r})$ can be obtained from the pseudo-wave-function $\tilde{\Psi}_{\mathbf{k}n}(\mathbf{r})$ according to the relation $\Psi_{\mathbf{k}n}(\mathbf{r})=\tilde{\Psi}_{\mathbf{k}n}(\mathbf{r})+\Psi^1_{\mathbf{k}n}(\mathbf{r})-\tilde{\Psi}^1_{\mathbf{k}n}(\mathbf{r})$ with

$$\Psi^1_{\mathbf{k}n}(\mathbf{r})-\tilde{\Psi}^1_{\mathbf{k}n}(\mathbf{r})=\sum_{a,i}\,[\Phi_i^a(\mathbf{r}-\mathbf{R^a})-\tilde{\Phi}_i^a(\mathbf{r}-\mathbf{R^a})]\langle\tilde{p}_i^a|\tilde{\Psi}_{\mathbf{k}n}\rangle, \tag{3}$$

where $\mathbf{R^a}$ denotes the atomic position of the atom a in the unit cell. It is useful to point out that $\Psi^1_{\mathbf{k}n}-\tilde{\Psi}^1_{\mathbf{k}n}$ vanishes in the interstitial region and defines the quantity necessary to describe the true wave function in the augmentation regions while $\tilde{\Psi}_{\mathbf{k}n}$ describes the true wave function in the interstitial region. It is, however, interesting to point out that, like in the pseudopotential method, the initial setups for producing the partial waves and the projector functions have to be optimized to obtain accurate LDA eigenvalues and eigenvectors (for more details see Ref. 31).

The PAW formalism is designed to easily calculate the expectation value of a local or a semilocal operator. For example, the expectation value of an operator $A(\mathbf{r})$ between two Bloch wave functions $\Psi_{\mathbf{k}n}$ and $\Psi_{\mathbf{k}m}$ can be expressed as a sum of three contributions

$$A_{n\mathbf{k},m\mathbf{k}}=\langle\Psi_{\mathbf{k}n}|A|\Psi_{m\mathbf{k}}\rangle=\tilde{A}_{n\mathbf{k},m\mathbf{k}}+A^1_{n\mathbf{k},m\mathbf{k}}-\tilde{A}^1_{n\mathbf{k},m\mathbf{k}}, \tag{4}$$

where the contribution $\tilde{A}_{n\mathbf{k},m\mathbf{k}}=\langle\tilde{\Psi}_{\mathbf{k}n}|A|\tilde{\Psi}_{\mathbf{k}m}\rangle$ is evaluated in the plane-wave basis set. The last two contributions

$$A^1_{n\mathbf{k},m\mathbf{k}}=\sum_{i,j,a}\,\langle\tilde{\Psi}_{\mathbf{k}n}|\tilde{p}_i^a\rangle\langle\Phi_i^a|A|\Phi_j^a\rangle\langle\tilde{p}_j^a|\tilde{\Psi}_{\mathbf{k}m}\rangle \tag{5}$$

and

$$\tilde{A}^1_{n\mathbf{k},m\mathbf{k}}=\sum_{i,j,a}\,\langle\tilde{\Psi}_{\mathbf{k}n}|\tilde{p}_i^a\rangle\langle\tilde{\Phi}_i^a|A|\tilde{\Phi}_j^a\rangle\langle\tilde{p}_j^a|\tilde{\Psi}_{\mathbf{k}m}\rangle \tag{6}$$

are computed in the augmentation regions. Minimizing the total energy with respect to the $\tilde{\Psi}_{\mathbf{k}n}$ (variational principle) leads to a generalized eigenvalue problem which is solved in a self-consistent way, giving the pseudo-wave-functions $\tilde{\Psi}_{\mathbf{k}n}$ from which the all-electron wave functions $\Psi_{\mathbf{k}n}$ are easily deduced by means of Eq. (3).

B. The all-electron *GW* approximation

1. Quasiparticle energies

In the QP approximation, the excitation energies of the system are obtained by solving a Schrödinger-like equation of the form

$$(T+V_{ext}+V_h)\Psi_{\mathbf{k}n}(\mathbf{r})+\int d^3r'\Sigma[\mathbf{r},\mathbf{r}',E_n(\mathbf{k})]\Psi_{\mathbf{k}n}(\mathbf{r}')=E_n(\mathbf{k})\Psi_{\mathbf{k}n}(\mathbf{r}), \tag{7}$$

instead of locating the poles of the Green's function. Here, T is the kinetic energy operator ($-\frac{1}{2}\nabla^2$ in atomic units), V_{ext} is the external (ionic) potential, V_h is the Hartree potential due to the average Coulomb repulsion of the electrons, and Σ is the self-energy operator that summarizes the many-body effects and is defined as $\Sigma(\mathbf{r},\mathbf{r}',\omega)=(i/2\pi)\int e^{i\delta\omega'}G(\mathbf{r},\mathbf{r}',\omega+\omega')W(\mathbf{r},\mathbf{r}',\omega')\mathrm{d}\omega'$, where G is the one-electron Green's function and W the screened interaction. Because it was shown[3] that the LDA wave function and the quasiparticle wave function have almost 99% overlap it is a good approximation to treat $\Sigma-V_{xc}^{LDA}$ as a perturbation (V_{xc}^{LDA} is the LDA valence exchange-correlation potential). The QP energies $E_n(\mathbf{k})$ can be written as

$$E_n(\mathbf{k})=\epsilon_n(\mathbf{k})+\langle\Psi_{\mathbf{k}n}|\Sigma[E_n(\mathbf{k})]|\Psi_{\mathbf{k}n}\rangle-\langle\Psi_{\mathbf{k}n}|V_{xc}^{LDA}(n_v)|\Psi_{\mathbf{k}n}\rangle, \tag{8}$$

where $\epsilon_n(\mathbf{k})$ is the LDA eigenvalue for band n. In principle, the solution to this equation should be obtained via an iterative method, but expanding Eq. (8) to first order in energy around $\epsilon_n(\mathbf{k})$ yields accurate numerical results of the QP energies

$$E_n(\mathbf{k})-\epsilon_n(\mathbf{k})=Z_{n\mathbf{k}}\{\langle\Psi_{\mathbf{k}n}|\Sigma[\epsilon_n(\mathbf{k})]|\Psi_{\mathbf{k}n}\rangle-\langle\Psi_{\mathbf{k}n}|V_{xc}^{LDA}(n_v)|\Psi_{\mathbf{k}n}\rangle\}, \tag{9}$$

TABLE I. The renormalization constants Z for the hole state at the valence-band maximum (VBM) and the electron state at the conduction- band maximum (CBM) for C, Si, GaAs, AlAs, InP, and $SiMg_2$.

	Diamond	Si	GaAs	AlAs	InP	Mg_2Si
Z_{VBM}	0.85	0.80	0.80	0.81	0.79	0.76
Z_{CBM}	0.87	0.81	0.81	0.82	0.82	0.79

where the QP renormalization factor $Z_{n\mathbf{k}}$ is

$$Z_{n\mathbf{k}}=\left[1-\langle\Psi_{\mathbf{k}n}|\frac{\partial}{\partial\omega}\Sigma(\omega)|_{\omega=\epsilon_n(\mathbf{k})}|\Psi_{\mathbf{k}n}\rangle\right]^{-1}. \quad (10)$$

Since $(\partial/\partial\omega)\Sigma<0$, we have $0<Z_{n\mathbf{k}}<1$ with typical values of 0.8 for bands close to the band gap and for all materials considered here (see Table I). Values of $Z_{n\mathbf{k}}$ about 0.8 imply that we still have well-defined QP in the system but that 20% of the spectral weight is now distributed over a range of frequencies.

2. Computation of the matrix elements of Σ within the PAW formalism

As can be seen from Eq. (9), the central problem of this scheme consists of evaluating the diagonal matrix elements of the self-energy between the LDA orbitals. The quantities that enter the self-energy are functions f of two locations $\mathbf{r}$ and $\mathbf{r}'$. These functions have the translational symmetry property $f(\mathbf{r}+\mathbf{R},\mathbf{r}'+\mathbf{R})=f(\mathbf{r},\mathbf{r}')$ where R is a Bravais lattice vector. Then, we can fix the Fourier transform convention for such functions

$$f(\mathbf{r},\mathbf{r}',\omega)=\frac{1}{\Omega}\sum_{\mathbf{q},\mathbf{G},\mathbf{G}'}e^{i(\mathbf{q}+\mathbf{G})\mathbf{r}}f_{\mathbf{G}\mathbf{G}'}(\mathbf{q},\omega)e^{-i(\mathbf{q}+\mathbf{G}')\mathbf{r}'}, \quad (11)$$

where $\mathbf{q}$ is a wave vector in the first BZ, $\mathbf{G}$ a reciprocal lattice vector, and Ω the crystal volume.

Using this convention, the dynamically screened interaction W that enters the expression of the self-energy is defined as

$$W_{\mathbf{G}\mathbf{G}'}(\mathbf{q},\omega)=\frac{4\pi}{\Omega}\frac{1}{|\mathbf{q}+\mathbf{G}|}\tilde{\epsilon}^{-1}_{\mathbf{G}\mathbf{G}'}(\mathbf{q},\omega)\frac{1}{|\mathbf{q}+\mathbf{G}'|}. \quad (12)$$

To compute this screened interaction and hence the self-energy, the symmetrized dielectric matrices $\tilde{\epsilon}_{\mathbf{G}\mathbf{G}'}(\mathbf{q},\omega)$ obtained within the RPA have to be calculated and inverted for many values of ω. This is computationally time consuming. Nevertheless, it has been carried out by some authors[5,14] who choose to evaluate the frequency integral by using a Gaussian integration scheme along the imaginary axis to circumvent the problem of the pole structure of the screened interaction along the real frequency axis.[5] An alternative approach is the use of a plasmon-pole model[3,9,12,32] to describe the frequency dependence of the dielectric matrix. These models give a good description of the low-frequency behavior of the dynamically-screened interaction and allow the determination of an analytic expression for the frequency integral appearing in the self-energy formula. We have used three types of plasmon-pole models to describe approximately the dependence of $\tilde{\epsilon}^{-1}(\omega)$ on the frequency ω. These different models were proposed by von der Linden and Horsch,[9] Engel and Farid,[32] and by Hamada *et al.*[12]

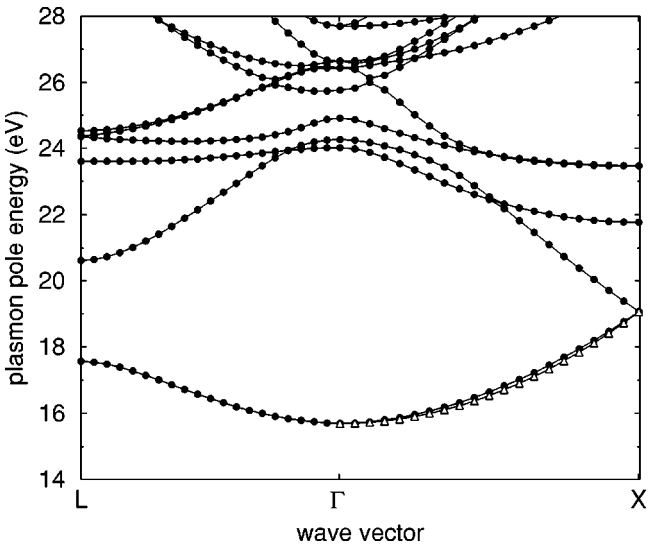

FIG. 1. PAW calculated Engel-Farid plasmon-pole model band structure of Si along $L\Gamma$ and ΓX high-symmetry directions. For small $\mathbf{k}$ wave vectors the lowest plasmon band shows a quadratic dispersion (up-triangle curve) $\omega_0(\mathbf{k})=\omega_0(\mathbf{0})+\alpha|\mathbf{k}|^2$, with a dimensionless direction-dependent dispersion coefficient α. Using a least-squares fit we find $\omega_0(\mathbf{0})=15.7$ eV and $\alpha=0.33$. These values are in good agreement with the corresponding Engel and Farid (Ref. 32) PP values of 15.91 eV and 0.34 as well as the experimental values (Ref. 36) of 16.7 eV and 0.41.

To test our implementation of the plasmon-pole model, we have plotted in Fig. 1 the Engel-Farid plasmon-pole model band structure of Si along the L, Γ, and X high-symmetry directions. We have found that our results are in excellent agreement with the results of Engel and Farid[32] and Aulbur.[35] Indeed, for small $\mathbf{k}$ wave vectors, the lowest plasmon band shows a quadratic dispersion $\omega_0(\mathbf{k})=\omega_0(\mathbf{0})+\alpha|\mathbf{k}|^2$, with a dimensionless direction-dependent dispersion coefficient α (see the fitted up-triangle curve in Fig. 1). For the ΓX direction our least-squares fit produced $\omega_0(\mathbf{0})=15.7$ eV and $\alpha=0.33$ in good agreement with the corresponding Engel and Farid's values of 15.91 eV and 0.34 (Ref. 32) as well as the experimental values of 16.7 eV and 0.41.[36] To also check the validity of the plasmon-pole model as a substitute for the dielectric function of real materials we have compared the plasmon-pole model of Hamada *et al.*[12] with our direct *ab initio* computation of the dielectric function within the RPA, including the so-called local-field effects (see Fig. 2) and with available experimental results[36] for the energy-loss spectrum. We notice that the model reproduces correctly our *ab initio* calculated dielectric function.

The matrix elements of the self-energy could be divided into an energy-independent contribution Σ^{HF} and an energy-dependent contribution $\Sigma(\omega)$. The first term corresponds to the Hartree-Fock contribution and is given by

$$\langle\Psi_{\mathbf{k}n}|\Sigma^{HF}|\Psi_{\mathbf{k}n}\rangle=-\frac{4\pi}{\Omega}\sum_{\mathbf{q}}\sum_{m\,occ}\sum_{\mathbf{G}}\frac{|M^{mn}_{\mathbf{G}}(\mathbf{k},\mathbf{q})|^2}{|\mathbf{q}+\mathbf{G}|^2}, \quad (13)$$

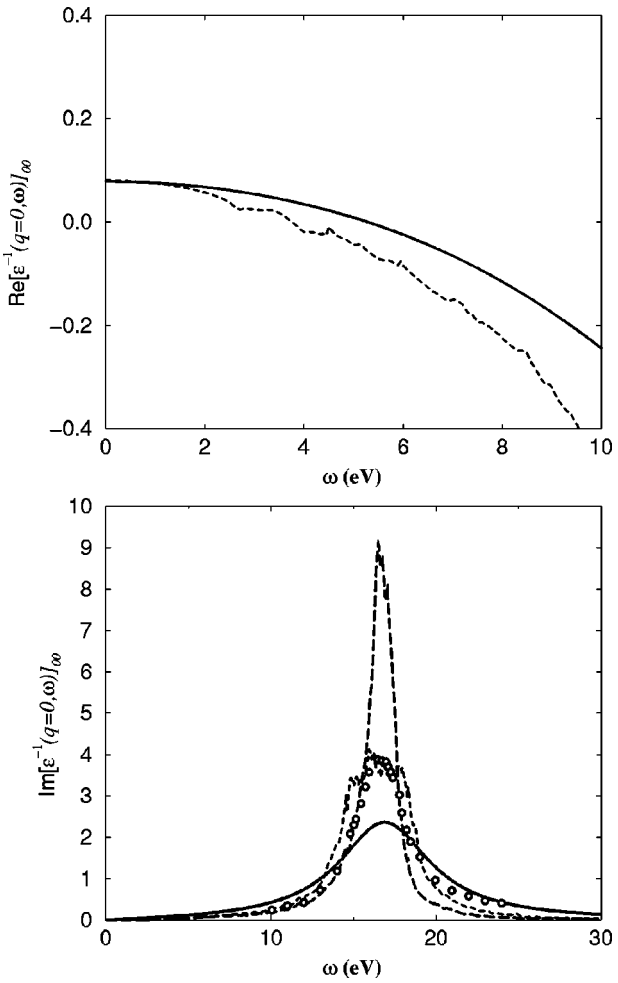

FIG. 2. *Ab initio* calculated real and imaginary parts of the inverse dielectric function (dashed curve) of Si compared with the plasmon-pole model of Hamada *et al.* (Ref. 12) (solid line) and with experiment (open circles) (Ref. 36). The long dashed curve is without the local-field effect.

where the summation runs only over the occupied states, and where $M_{\mathbf{G}}^{nm}(\mathbf{k},\mathbf{q})=\langle\Psi_{\mathbf{k}-\mathbf{q}n}|e^{-i(\mathbf{q}+\mathbf{G})\cdot\mathbf{r}}|\Psi_{\mathbf{k}m}\rangle$. Using the von der Linden–Horsch plasmon-pole model, the energy-dependent contribution can be expressed as

$$\langle\Psi_{\mathbf{k}n}|\Sigma(\omega)|\Psi_{\mathbf{k}n}\rangle = \frac{4\pi}{\Omega}\sum_{\mathbf{q},m,p} \times\frac{z_p(\mathbf{q})\omega_p(\mathbf{q})/2}{\omega-\epsilon_m(\mathbf{k}-\mathbf{q})+[\omega_p(\mathbf{q})-i\delta]\mathrm{sgn}[\mu-\epsilon_m(\mathbf{k}-\mathbf{q})]} \times|\beta_p^{mn}(\mathbf{k},\mathbf{q})|^2, \tag{14}$$

where ω_p and z_p are the frequency and the force of the pole, respectively. Here β_p^{mn} is given by

$$\beta_p^{mn}(\mathbf{k},\mathbf{q})=\sum_{\mathbf{G}}[M_{\mathbf{G}}^{mn}(\mathbf{k},\mathbf{q})]^*\frac{\phi_{p\mathbf{q}}(\mathbf{G})}{|\mathbf{q}+\mathbf{G}|}, \tag{15}$$

where m and n are energy band indexes, p is a plasmon-band index, and $\mathbf{q}$ is a vector in the BZ. The $\phi_{p\mathbf{q}}(\mathbf{G})$ are the Fourier components of the eigenvectors of the static dielectric function $\tilde{\epsilon}_{\mathbf{G},\mathbf{G}'}(\mathbf{q},\omega=0)$. It should be emphasized that the summation over m is not restricted to occupied states as in the expression of the Hartree-Fock contribution. Both the poles of the Green's function and of the screened interaction contribute to this expression. The expression of the energy-dependent contribution of Σ using the other two plasmon-pole models can be found elsewhere.[17–19] We emphasize that the QP energies are not too sensitive to the type of the plasmon-pole model used.

3. Numerical details

One of the central problems within the realization of the GWA is the calculation of matrix elements $M_{\mathbf{G}}^{nm}(\mathbf{k},\mathbf{q})$. Using the PAW formalism, the smooth pseudo-wave-function $\tilde{\Psi}_{\mathbf{k}n}$ associated with an ''all-electron'' LDA wave function $\Psi_{\mathbf{k}n}$ is defined as

$$\tilde{\Psi}_{\mathbf{k}n}(\mathbf{r})=\frac{1}{\sqrt{V}}\sum_{\mathbf{G}}A_{\mathbf{k}n}(\mathbf{G})e^{i(\mathbf{k}+\mathbf{G})\mathbf{r}}, \tag{16}$$

where the sum runs over the reciprocal-lattice vectors. As illustrated in the part dedicated to the PAW formalism, the expectation value of $e^{-i(\mathbf{q}+\mathbf{G})\cdot\mathbf{r}}$ can be divided into three parts,

$$M_{\mathbf{G}}^{nm}(\mathbf{k},\mathbf{q})=\langle\tilde{\Psi}_{\mathbf{k}-\mathbf{q}n}|e^{-i(\mathbf{q}+\mathbf{G})\mathbf{r}}|\tilde{\Psi}_{\mathbf{k}m}\rangle +\langle\Psi^1_{\mathbf{k}-\mathbf{q}n}|e^{-i(\mathbf{q}+\mathbf{G})\mathbf{r}}|\Psi^1_{\mathbf{k}m}\rangle -\langle\tilde{\Psi}^1_{\mathbf{k}-\mathbf{q}n}|e^{-i(\mathbf{q}+\mathbf{G})\mathbf{r}}|\tilde{\Psi}^1_{\mathbf{k}m}\rangle. \tag{17}$$

The first term, which involves plane waves, is defined as

$$\sum_{\mathbf{G}'}A^*_{\mathbf{k}-\mathbf{q}n}(\mathbf{G}')A_{\mathbf{k}m}(\mathbf{G}+\mathbf{G}'). \tag{18}$$

In this expression the summation over the reciprocal-lattice vectors is limited to all vectors $\mathbf{G}'$ such that both the absolute values of $\mathbf{G}'$ and $\mathbf{G}+\mathbf{G}'$ are smaller than a cutoff parameter. In general $300\mathbf{G}'$ vectors were included in the summation for the systems studied here, except for Mg_2Si and diamond where the convergence is achieved only when 645 and $400\mathbf{G}'$ vectors were used, respectively. The two remaining terms that involve localized contributions can be expressed as

$$\sum_{\mathbf{a},i,j}\langle\tilde{\Psi}_{\mathbf{k}-\mathbf{q}n}|\tilde{p}_j^{\mathbf{a}}\rangle[\langle\Phi_j^{\mathbf{a}}|e^{-i(\mathbf{q}+\mathbf{G})\mathbf{r}}|\Phi_i^{\mathbf{a}}\rangle -\langle\tilde{\Phi}_j^{\mathbf{a}}|e^{-i(\mathbf{q}+\mathbf{G})\mathbf{r}}|\tilde{\Phi}_i^{\mathbf{a}}\rangle]\langle\tilde{p}_i^{\mathbf{a}}|\tilde{\Psi}_{m\mathbf{k}}\rangle. \tag{19}$$

Since the overlap between the pseudo-wave-functions and the projectors is known, we have to calculate quantities like $\langle\Phi_j^{\mathbf{a}}|e^{-i(\mathbf{q}+\mathbf{G})\cdot\mathbf{r}}|\Phi_i^{\mathbf{a}}\rangle$. By expanding a plane wave on spherical Bessel functions j_l, we obtain

$$\langle \Phi_j^{\mathbf{a}} | e^{-i(\mathbf{q}+\mathbf{G})\mathbf{r}} | \Phi_i^{\mathbf{a}} \rangle = 4\pi e^{-i(\mathbf{q}+\mathbf{G})\mathbf{R_a}} \sum_{lm} (-i)^l Y_{lm}(\widehat{\mathbf{q}+\mathbf{G}}) G^{lm}_{l_i m_i\, l_j m_j} \times \int_0^{r_c^{\mathbf{a}}} dr\, r^2 j_l(|\mathbf{q}+\mathbf{G}||\mathbf{r}|) \Phi_{l_j n_j}(r) \times \Phi_{l_i n_i}(r), \quad (20)$$

where the Gaunt coefficients are given by

$$G^{lm}_{l_i m_i\, l_j m_j} = \sqrt{4\pi} \int d\Omega\, Y^*_{l_i m_i}(\hat{\mathbf{r}}) Y^*_{lm}(\hat{\mathbf{r}}) Y_{l_j m_j}(\hat{\mathbf{r}}). \quad (21)$$

The symmetrized dielectric matrix as well as the matrix elements of the self-energy defined by Eqs. (13) and (14) are obtained by an integration over the BZ using the special points' technique.[37] The summation over $\mathbf{q}$ points in the expectation value of the self-energy has to be carried out carefully, since the integrands have an integrable singularity in $1/\mathbf{q}^2$ for $\mathbf{q}\to 0$. This can be readily seen in the expectation value of Σ^{HF} defined by Eq. (13) where the divergence occurs when $\mathbf{G}=0$. To integrate out the singularity we followed a procedure developed by Gygi and Baldereschi.[38] This procedure consists of adding and removing a smooth function $F(\mathbf{q})$ which reflects the translational symmetry of the Bravais lattice and which diverges as $1/\mathbf{q}^2$ as $\mathbf{q}$ vanishes. For example, the Hartree-Fock contribution can be written as

$$\langle \Psi_{\mathbf{k}n} | \Sigma^{HF} | \Psi_{\mathbf{k}n} \rangle = -\frac{4\pi}{\Omega} \sum_q \sum_{m\, occ} \left[\sum_{\mathbf{G}} \frac{|M^{mn}_{\mathbf{G}}(\mathbf{k},\mathbf{q})|^2}{|\mathbf{q}+\mathbf{G}|^2} - F(\mathbf{q})\delta_{mn} \right] - \frac{4\pi}{\Omega} \sum_{m\, occ} \delta_{mn} \sum_q F(\mathbf{q}). \quad (22)$$

The function in square brackets does not contain any divergence due to the fact that $\lim_{\mathbf{q}\to 0} M^{mn}_{\mathbf{0}}(\mathbf{k},\mathbf{q}) = \delta_{mn}$, and it is easily integrated using the special points method while the integral of $F(\mathbf{q})$ over the BZ is performed analytically.

The development of $|\beta^{mn}_p(\mathbf{k},\mathbf{q})|^2$ in Eq. (14) shows two types of divergence, see Eq. (15). The first is of $1/\mathbf{q}^2$ type and is treated using a method similar to that given by Eq. (22), while the second one is of $1/|\mathbf{q}|$ type and can be solved using another type of analytical function which diverges as $1/|\mathbf{q}|$ when $\mathbf{q}\to 0$. Nevertheless, we have found that this latter divergence is less severe than the former and does not require a special treatment since the accuracy of the numerical results is not affected if it is neglected. It should be noted that the treatment of the singularity in Eq. (14) requires the evaluation of the symmetrized dielectric matrix for $\mathbf{q}\to 0$. As the convergence of the head element of this matrix as a function of the number of $\mathbf{k}$ points is slow, the calculation is performed separately. All other BZ integrations are carried out using ten special $\mathbf{k}$ points in the final calculations producing well converged results (see Sec. III).

The computation of the QP energies requires the determination of the renormalization factor defined by Eq. (10). The derivative of the self-energy is then calculated using a finite difference scheme with a step of 1 eV. The values of the renormalization factors are summarized in Table I for the different materials studied here. These Z values are roughly the same for the electron and hole states, and for all the materials studied in this paper. The deviation from unity of the Z values indicates that their correct determination is crucial for obtaining accurate QP energies. It is worth noticing that values of Z closer to unity imply that the quasiparticles are well defined and that the GWA is a reasonable approximation.

4. The decoupling of the core and valence electrons

The last point to be discussed is the decoupling of the core and valence electrons so that when computing the QP energies using Eq. (8) the appropriate valence-electron exchange-correlation matrix elements are subtracted out. It is clear that this subtracting procedure may be a source of inaccuracy due to the nonlinearity of the exchange-correlation potential $V^{LDA}_{xc}[n(\mathbf{r})] = V^{LDA}_{xc}[n_c(\mathbf{r}) + n_v(\mathbf{r})]$ with respect to the total charge density n, where n_c and n_v are the core and the valence densities, respectively. For this reason we have tested two different schemes for decoupling the core and valence electrons. In the first scheme we assumed that the core-valence exchange-correlation and core-polarization contributions to the energy of a valence state are given by[3]

$$\langle \Psi_{\mathbf{k}n} | V_{xc\ \mathrm{core-val}} | \Psi_{\mathbf{k}n} \rangle = \langle \Psi_{\mathbf{k}n} | V_{xc}[n_v + n_c] | \Psi_{\mathbf{k}n} \rangle - \langle \Psi_{\mathbf{k}n} | V_{xc}[n_v] | \Psi_{\mathbf{k}n} \rangle. \quad (23)$$

Such a procedure is somewhat hidden when pseudopotentials are used since such an operation is performed in the unscreening of the pseudopotential by subtracting $V_{xc}[n_v]$. The shortcoming of this approach is that the ionic pseudopotential is dependent on the valence configuration, reducing the transferability of the potential. In addition, it has been shown that including core corrections to the exchange and correlation is necessary for the correct description of the structural properties of solids.[39] The PAW does not suffer from this shortcoming but it seems that justifying Eq. (23) is not an easy task. Assuming that the argument mentioned above is approximatively correct, the quantity which must be subtracted is then defined by

$$\langle \Psi_{\mathbf{k}n} | V^{LDA}_{xc}[n_v(\mathbf{r})] | \Psi_{\mathbf{k}n} \rangle = \langle \tilde{\Psi}_{\mathbf{k}n} | V^{LDA}_{xc}[\tilde{n}_v(\mathbf{r})] | \tilde{\Psi}_{\mathbf{k}n} \rangle + \sum_{i,j,a} \langle \tilde{\Psi}_{n\mathbf{k}} | \tilde{p}^a_i \rangle \times \{ \langle \Phi^a_i | V^{LDA}_{xc}[n^1_v(\mathbf{r})] | \Phi^a_j \rangle - \langle \tilde{\Phi}^a_i | V^{LDA}_{xc}[\tilde{n}^1_v(\mathbf{r})] \times | \tilde{\Phi}^a_j \rangle \} \langle \tilde{p}^a_j | \tilde{\Psi}_{n\mathbf{k}} \rangle. \quad (24)$$

The other scheme for decoupling the core and valence electrons consists of computing directly the core-valence exchange interaction within the Hartree-Fock approximation.[2,40] The density matrix $\rho_c(\mathbf{r},\mathbf{r}')$ of the core state is defined as

$$\rho_c(\mathbf{r},\mathbf{r}') = \sum_{a,n_c,l_c,m_c} \Psi^a_{n_c l_c m_c}(\mathbf{r}) \Psi^{a\star}_{n_c l_c m_c}(\mathbf{r}'), \quad (25)$$

TABLE II. Matrix elements of the exchange-correlation potential of the valence states $\langle\Psi_{\mathbf{k}n}|V_{xc}^{LDA}[n_v]|\Psi_{\mathbf{k}n}\rangle$ compared with exchange-correlation of the total charge minus the core exchange potential within the Hartree-Fock approximation $\langle\Psi_{\mathbf{k}n}|V_{xc}^{LDA}[n_v+n_c]|\Psi_{\mathbf{k}n}\rangle-\langle\Psi_{\mathbf{k}n}|V_X^c|\Psi_{\mathbf{k}n}\rangle$ for Si (in eV). The resulting QP energies at the high-symmetry points are also compared. Here $E_{QP}^{(1)}$ is obtained using $\langle\Psi_{\mathbf{k}n}|V_{xc}^{LDA}[n_v+n_c]|\Psi_{\mathbf{k}n}\rangle-\langle\Psi_{\mathbf{k}n}|V_X^c|\Psi_{\mathbf{k}n}\rangle$ instead of $\langle\Psi_{\mathbf{k}n}|V_{xc}^{LDA}[n_v(\mathbf{r})]|\Psi_{\mathbf{k}n}\rangle$ in Eq. (8) while $E_{QP}^{(2)}$ is obtained using the standard procedure defined in Eq. (8). The average deviation of the two types of QP calculations is less than 0.1 eV suggesting that the LDA exchange and correlation of the valence electrons is well subtracted out from the GWA self-energy.

	V_X^c	$V_{xc}[n_v+n_c]$	$V_{xc}[n_v+n_c]-V_X^c$	$V_{xc}[n_v]$	$E_{QP}^{(1)}$	$E_{QP}^{(2)}$
Γ_{1v}	−1.40	−12.01	−10.61	−10.57	−12.05	−11.96
$\Gamma_{25'v}$	−1.85	−13.45	−11.60	−11.45	0.0	0.0
Γ_{15c}	−1.40	−11.74	−10.34	−10.19	3.15	3.15
$\Gamma_{2'c}$	−4.15	−15.41	−11.26	−11.16	4.15	4.19
X_{1v}	−1.79	−12.81	−11.02	−10.95	−7.99	−7.92
X_{4v}	−1.52	−12.37	−10.85	−10.74	−3.05	−3.01
X_{1c}	−0.92	−10.17	−9.25	−9.15	1.10	1.15
X_{3c}	−2.81	−13.90	−11.09	−10.84	10.81	10.75
$L_{2'v}$	−1.70	−12.71	−11.01	−10.95	−9.76	−9.61
L_{1v}	−1.40	−11.81	−10.41	−10.33	−7.24	−7.17
$L_{3'v}$	−1.78	−13.11	−11.33	−11.20	−1.28	−1.26
L_{1c}	−2.26	−12.65	−10.39	−10.28	2.12	2.16
L_{3c}	−0.97	−10.89	−9.92	−9.78	3.94	3.95

where $\Psi^a_{n_c l_c m_c}(\mathbf{r})=\Phi_{n_c l_c}(|\mathbf{r}-\mathbf{R}^a|)Y_{l_c m_c}(\widehat{\mathbf{r}-\mathbf{R}^a})$ is a core state centered at site $\mathbf{R}^a$ of principal quantum number n_c, angular quantum number l_c, and magnetic number m_c.

The exchange operator of the core state is defined as

$$V_X^c(\mathbf{r},\mathbf{r}')=-\frac{\rho_c(\mathbf{r},\mathbf{r}')}{|\mathbf{r}-\mathbf{r}'|}. \tag{26}$$

It is then possible to calculate accurately the core-valence exchange if we assume that the LDA core wave function and the Hartree-Fock one are similar. In fact, the core states, and in particular the partial wave and pseudo-partial-waves, which are the basic ingredients of the PAW method, are obtained from an atomic all-electron calculation within the LDA. The matrix elements of the core-valence exchange are then defined as

$$\langle\Psi_{m\mathbf{k}}|V_X^c|\Psi_{n\mathbf{k}}\rangle=-\sum_{a,n_c,l_c,m_c}\int_{S_a}d^3r\,d^3r'\times\frac{\Psi^{\star}_{m\mathbf{k}}(\mathbf{r})\Psi^a_{n_c l_c m_c}(\mathbf{r})\Psi^{a^{\star}}_{n_c l_c m_c}(\mathbf{r}')\Psi_{n\mathbf{k}}(\mathbf{r}')}{|\mathbf{r}-\mathbf{r}'|}. \tag{27}$$

We take advantage of the fact that the core states are well described as closed shells and that in the augmentation region the Bloch wave function $\Psi_{n\mathbf{k}}(\mathbf{r})$ is correctly described using an atomic wave-function expansion

$$\Psi_{n\mathbf{k}}(\mathbf{r})=\sum_{a,i}\Phi_i^a(\mathbf{r}-\mathbf{R}^{\mathbf{a}})\langle\tilde{p}_i^a|\tilde{\Psi}_{n\mathbf{k}}\rangle\quad\text{for}\quad|\mathbf{r}-\mathbf{R}^{\mathbf{a}}|\leqslant r_c^a \tag{28}$$

to rewrite the core-valence exchange matrix elements as

$$\langle\Psi_{m\mathbf{k}}|V_X^c|\Psi_{n\mathbf{k}}\rangle=\sum_K\left[\frac{(2l_c+1)(2l+1)}{4\pi(2l_i+1)}\right]^{1/2}\times C^{l_i 0}_{l\,0\,l_c 0}\langle\tilde{p}^a_{n_i l_i m_i}|\tilde{\Psi}_{m\mathbf{k}}\rangle^*\langle\tilde{p}^a_{n_j l_i m_i}|\tilde{\Psi}_{n\mathbf{k}}\rangle\times I^a(n_i,n_j,n_c,l_c,l), \tag{29}$$

where $K=(a,n_i,n_j,n_c,l_c,l_i,m_i,l)$ and the radial integrals $I^a(n_i,n_j,n_c,l_c,l)$ are defined by

$$I^a(n_i,n_j,n_c,l_c,l)=\int_0^{R^a}r^2dr\int_0^{R^a}r'^2dr'\Phi^a_{n_c l_c}(r)\Phi^a_{n_i l_i}(r)G_l(r,r')\times\Phi^a_{n_c l_c}(r')\Phi^a_{n_j l_i}(r'), \tag{30}$$

where G_l is given by

$$G_l(r,r')=\frac{4\pi}{2l+1}\frac{r_<^l}{r_>^{l+1}}. \tag{31}$$

Here $r_<$ ($r_>$) is the smaller (greater) of r and r'.

In Table II we compare the matrix elements of the valence exchange-correlation matrix elements $\langle\Psi_{\mathbf{k}n}|V_{xc}^{LDA}[n_v]|\Psi_{\mathbf{k}n}\rangle$ with that of the total density minus that of the core-valence exchange $\langle\Psi_{\mathbf{k}n}|V_{xc}^{LDA}[n_v+n_c]|\Psi_{\mathbf{k}n}\rangle-\langle\Psi_{\mathbf{k}n}|V_X^c|\Psi_{\mathbf{k}n}\rangle$ for Si. It is surprising that the two types of exchange-correlation matrix elements are found to be in good agreement to within 0.1 eV on average, and the resulting QP energies differ by less than 0.1 eV on average.

TABLE IV. Calculated differences of the LDA matrix elements of the exchange-correlation potential $\Delta\langle\Psi_{\mathbf{k}n}|V_{xc}^{LDA}[n_v]|\Psi_{\mathbf{k}n}\rangle$, the self-energy $\Delta\Sigma(E_{qp})$, as well as its Hartree-Fock contribution $\Delta\Sigma^{HF}$ of silicon compared with the LAPW of Hamada *et al.* (Ref. 12) and PP results of Olevano (Ref. 41) and Shirley (Ref. 42) (in parentheses). Concerning the ΔV_{xc} our results are in good agreement with the LAPW results (Ref. 12) and disagree with the PP calculations at the *X* point. This discrepancy of about 0.17 eV makes the PP-GWA indirect band gap at least 0.17 eV larger than the ours explaining the difference between the PP-GWA and PAW-GWA indirect band gaps. For the $\Delta\Sigma^{HF}$ and $\Delta\Sigma$ our data agree nicely with the PP calculations of Olevano (Ref. 41) and somewhat less with that of Shirley (Ref. 42) and even less with the LAPW results (Ref. 12).

	ΔV_{xc}			$\Delta\Sigma^{HF}$			$\Delta\Sigma(E_{qp})$		
	Present	LAPW [a]	PP [b]	Present	LAPW [a]	PP [b]	Present	LAPW [a]	PP [b]
$\Gamma'_{25v}\rightarrow\Gamma_{15c}$	1.26	1.22	1.20 (1.20)	6.70	7.59	6.66 (6.92)	1.87	1.97	1.89 (2.03)
$\Gamma'_{25v}\rightarrow X_{1c}$	2.30	2.24	2.13 (2.14)	7.22	8.07	7.17 (7.48)	2.77	2.73	2.85 (2.92)
$\Gamma'_{25v}\rightarrow L_{1c}$	1.17	1.11	1.13 (1.15)	6.42	7.34	6.41 (6.70)	1.79	1.84	1.80 (1.96)

[a]Reference 12.
[b]Reference 41.

III. QUASIPARTICLE RESULTS AND DISCUSSION

A. Quasiparticle results of small- and medium-band-gap semiconductors: Si, GaAs, AlAs, InP, and Mg_2Si

In this section we present the electronic structure of several small- and medium-band-gap semiconductors which are used to test our implementation of the all-electron PAW-GWA method. As mentioned earlier we have implemented three different types of plasmon-pole models available in the literature[9,12,32] and compared in Table III the resulting QP energies of Si at the Γ, *L*, and *X* high-symmetry points of the BZ. This table shows that the Si QP energies are not sensitive to the type of plasmon-pole model used to describe the frequency dependence of the screened interaction. We have obtained similar results for the other semiconductors studied in this paper (see Tables V and VII). This behavior was also observed by Hedin[2] using a jellium model.

To test further our method we have made a detailed comparison with the only available full-potential GWA calculation of Si based on the linearized augmented-plane-wave method[12] (LAPW) and with various pseudopotential (PP) results.[41,42] To make this comparison with the LAPW reliable, we have used the plasmon-pole model of Hamada *et al.*[12] Table IV compares different key ingredients necessary to determine the QP energies of Si in the GWA. In particular, our calculated valence exchange-correlation potential matrix elements are compared with the LAPW-GWA (Ref. 12) and PP-GWA results.[41,42] The agreement between our exchange-correlation matrix elements and those of Hamada *et al.*[12] is remarkably good even though these results are based on different methods and that different parametrization of the exchange-correlation potential is used. However, concerning the comparison with PP results[41,42] we observe a significant discrepancy of about 0.17 eV at the *X* high-symmetry point. This discrepancy will be used later to explain the differences between the PP and PAW-GWA indirect band gap of Si which occurs at the vicinity of the *X* point. Concerning the Hartree-Fock contribution to the self-energy the agreement with the results of Hamada *et al.*[12] is less satisfactory. However, we found it surprising that our Hartree-Fock contribution to the self-energy is closer to the results of Olevano[41] and to some extent to these of Shirley[42] even though their calculations are of pseudopotential type. The successful comparison of the PP results makes us confident with our PAW-GWA results, and confirms the fact that the detailed structure of the screened interaction is not crucial for the correct determination of the QP energies. It is also surprising that the values of Σ obtained using the PAW or the LAPW implementation are close despite that the Hartree-Fock term did not agree.

To calculate the QP energies it is important to correctly determine the QP renormalization factor $Z_{n\mathbf{k}}$ [see Eq. (10)]. Table I presents $Z_{n\mathbf{k}}$ calculated for the top valence state at the Γ point and for the lowest conduction state of all semiconductors studied in this paper. These values are in good agreement with the results of Hybertsen and Louie[3] and they seem to be material and state independent and are about 0.8.

Tables V and VI show the calculated PAW-LDA and PAW-GWA band energies[43] for the high-symmetry points Γ, *X*, and *L* for small- and medium-band-gap semiconduc-

TABLE III. Quasiparticle (QP) energies of Si for several states (in eV) and for three different types of plasmon-pole models. We notice that the QP energies are less sensitive to the type of plasmon-pole model used. E_g is the indirect band gap.

	Plasmon-pole model		
	von der Linden and Horsch[a]	Hamada *et al.*[b]	Engel-Farid[c]
Γ_{1v}	−11.96	−11.95	−11.84
$\Gamma_{25'v}$	0.00	0.00	0.00
Γ_{15c}	3.15	3.13	3.17
$\Gamma_{2'c}$	4.19	4.17	4.16
X_{1v}	−7.92	−7.91	−7.85
X_{4v}	−3.01	−3.01	−2.97
X_{1c}	1.15	1.12	1.20
$L_{2'v}$	−9.67	−9.67	−9.59
L_{1v}	−7.17	−7.17	−7.08
$L_{3'v}$	−1.26	−1.27	−1.25
L_{1c}	2.16	2.14	2.17
L_{3c}	3.95	3.93	3.98
E_g	1.00	0.98	1.05

[a]Reference 9.
[b]Reference 12.
[c]Reference 32.

TABLE V. Quasiparticle band gaps of Si, GaAs, AlAs, and InP at Γ,L, and X points (in eV). The calculation of the self-energy is performed using ten special **k** points in the BZ and 200 bands. The size of the polarizability matrix is 137×137 for Si, 169×169 for the other semiconductors. The number of reciprocal-lattice vectors is 283 for Si, 307 for GaAs and AlAs, and 331 for InP. The QP GWA results are obtained using the plasmon-pole model of von der Linden and Horsch (Ref. 9) or that of Engel-Farid (results are in parentheses). Here E_g is the indirect band gap of Si; all band gaps are underlined. Our results are compared with the LAPW, PP, and experimental results.

	LDA			GWA			Expt.[c]
	Present	LAPW [a]	PP [b]	Present	LAPW [a]	PP [b]	
Si							
$\Gamma'_{25v}\rightarrow\Gamma_{1c}$	2.53	2.55	2.57 [d]; 2.57 [e]	3.15 (3.17)	3.30	3.35 [d]; 3.25 [e]	3.40; 3.05 [j]
$\Gamma'_{25v}\rightarrow X_{1c}$	0.65	0.65	0.6 [d]; 0.62 [e]	1.15 (1.20)	1.14	1.44 [d]; 1.33 [e]	1.25 [j]
$\Gamma'_{25v}\rightarrow L_{1c}$	1.52	1.43	1.51 [d]; 1.63 [e]	2.16 (2.17)	2.15	2.27 [d]; 2.28 [e]	2.1 [f], 2.4±0.15
E_g	0.50	0.52	0.52	1.00(1.05)	1.01	1.29 [d]	1.17
GaAs							
$\Gamma'_{25v}\rightarrow\Gamma_{1c}$	0.38		0.40	1.09(1.10)		1.29	1.52
$\Gamma'_{25v}\rightarrow X_{1c}$	1.29		1.18	1.64 (1.74)		2.05	1.90
$\Gamma'_{25v}\rightarrow L_{1c}$	0.89		0.83	1.45 (1.50)		1.69	1.73
AlAs							
$\Gamma'_{25v}\rightarrow\Gamma_{1c}$	1.95		1.77	2.83 (2.85)		2.75	3.11[g]
$\mathbf{\Gamma}'_{25v}\rightarrow\mathbf{X}_{1c}$	1.26		1.20	1.81(1.93)		2.08	2.24
$\Gamma'_{25v}\rightarrow L_{1c}$	2.07		1.89	2.83 (2.90)		2.79	2.49 [g]; 2.54 [h]
InP							
$\Gamma'_{25v}\rightarrow\Gamma_{1c}$	0.77		0.50	1.54(1.57)		1.23[k]	1.46 [i]
$\Gamma'_{25v}\rightarrow X_{1c}$	1.66		1.64	2.13 (2.27)		2.60 [k]	2.42 [i]
$\Gamma'_{25v}\rightarrow L_{1c}$	1.57		1.30	2.28 (2.36)		1.97 [k]	2.32 [i]

[a]Reference 12.
[b]Unless noted, Ref. 16.
[c]Unless noted, Ref. 44.
[d]Reference 3.
[e]References 41.
[f]Reference 49.
[g]Reference 51.
[h]Reference 52.
[i]Reference 53.
[j]Reference 45.
[k]Reference 13.

tors: Si, GaAs, AlAs, InP, and Mg_2Si, respectively. We have presented only the conduction states since the valence state energies are in good agreement with previous GWA calculations.[3,7,13,16,41,42,60] These results are compared with other GWA calculations obtained using LAPW (for Si) or PP for the other systems and to available experimental results.[44–55] Notice that the experimental results of Ref. 45 are based on inverse photoemission and seem to underestimate the direct band gap of Si at the Γ point.

The discrepancy between our GWA values and others is traced back mainly to differences between the LDA exchange-correlation matrix elements and to differences in the LDA eigenvalues. To support our claim we write the indirect band gap E_g of Si as roughly the difference between the conduction QP energy of the state X_{1c} and the valence QP of the state Γ'_{25v}. Using Eq. (8) this band gap can be expressed as the difference between the eigenvalues plus the difference between the self-energies minus the difference between the exchange-correlation matrix elements at X and Γ:

$$E_g=\epsilon(X_{1c})-\epsilon(\Gamma'_{25v})+\Sigma[E(X_{1c})]-\Sigma[E(\Gamma'_{25v})]-[V_{xc}^{LDA}(X_{1c})-V_{xc}^{LDA}(\Gamma'_{25v})]. \quad (32)$$

In fact this formula applies to all the direct and indirect band gaps. To determine quantitatively the effect of the LDA exchange-correlation matrix elements and the LDA eigenvalues we have determined the three band gaps of Si using our calculated self-energy and the PP-LDA eigenvalues and exchange-correlation matrix elements of Olevano[41] from Tables IV and V. The resulting band gaps are 3.24, 1.26, and 2.29 eV at Γ, X, and L, respectively, in good agreement with the PP calculations. This led us to the conclusion that the exchange-correlation matrix elements and the eigenvalues obtained using the PP method have a tendency to increase the band gaps by as much as 10% compared with the PAW results. This is nevertheless only true for small-band-gap semiconductors. For wide-band-gap semiconductors the deviation between the PAW-GWA and the PP-GWA is found not to exceed 3%. It was shown that for small- and medium-band-gap semiconductors having semicore states, like GaAs and AlAs, the addition of the core-polarization interaction improves their energy band gaps.[16] However, this formalism is computationally involved, and has been implemented only by Shirley and co-workers.[16]

Figure 3 presents the band structure of Si, GaAs, AlAs, InP, and Mg_2Si along the $L\Gamma$ and ΓX high-symmetry directions calculated using the LDA and GWA. We notice an overall improvement of the excited-state QP energies compared with those obtained in the LDA, whereas the LDA valence state eigenvalues are in general in good agreement with experiment and the GWA results do not change this agreement. In all these small- and medium-band-gap semiconductors we observe, as in previous PP-GWA calculations, that there is an almost rigid energy shift of the conduction

TABLE VI. Quasiparticle energies of Mg_2Si at some high-symmetry points. The calculation of the self-energy is performed using two special **k** points, 200 bands, and 645 reciprocal-lattice vectors. The size of the polarizability matrix is 113×113 and the plasmon-pole model of von der Linden and Horsch (Ref. 9) is used.

	LDA	GW approximation	Expt.[55]
Γ_{1v}	−9.19	−8.82	
Γ_{15v}	0.00	0.00	0.00
Γ_{1c}	1.55	2.15	2.1
Γ'_{25c}	2.41	2.84	
X_{1v}	−7.17	−6.91	
X'_{4v}	−4.46	−4.67	
X'_{5v}	−1.99	−2.14	
X_{3c}	0.12	0.45	
X_{1c}	0.20	0.62	
L_{1v}	−7.71	−7.45	
L'_{2v}	−4.79	−5.02	
L'_{3v}	−0.73	−0.78	
L_{1c}	0.98	1.50	
L_{3c}	2.44	2.84	
$L'_{3v}\rightarrow L_{3c}$	3.17	3.62	3.7
$X'_{5v}\rightarrow X_{1c}$	2.19	2.76	2.5
E_g	0.12	0.45	0.7−0.80

states towards higher energies with respect to the corresponding LDA values. This energy shift is about the same for Si and GaAs and is about 0.6 eV, and increases to about 0.8 eV for AlAs and InP.

To study the range of applicability of the so-called scissors-operator shift, which consists of rigidly shifting the conduction bands upwards, we calculated the energy dispersion of the difference between the LDA and the GWA direct band gaps across the BZ. For the scissors-operator shift to be valid, the difference between the GWA and LDA band gaps should be independent of **k**. However, our calculation shows that the scissor operator is accurate to about 0.06 and 0.04 for Si and Mg_2Si, respectively, and to about 0.16, 0.15, and 0.13 eV for GaAs, AlAs, and InP, respectively. These small deviations indicate that the GWA does not change much the LDA dispersion across the BZ, justifying the use of the scissors-operator shift for the calculation of the dielectric function for small- and medium-band-gap semiconductors.[56–58] In Sec. III B we show that these deviations are much larger for wide-band-gap semiconductors.

As for Mg_2Si we believe that it is the first time that this compound is studied within the GWA. The PAW-LDA and PAW-GWA QP energies for the high-symmetry points Γ, X, and L are shown in Table VI. Due to the lack of photoemission experiments, the GWA results are compared with optical measurements, making the assumption that excitonic effects are negligible. The GWA results are in good agreement with the experimental results and compare well with the empirical PP calculation of Au-Yang *et al.*[59] Figure 3 presents the corresponding band structure along the $L\Gamma$ and ΓX high-symmetry directions within the LDA and GWA.

TABLE VII. Quasiparticle band gaps of diamond and LiCl at Γ, L, and X (in eV). The calculation of the self-energy is performed using ten special **k** points in the BZ and 200 bands. The size of the polarizability matrix is 169×169 for diamond and 259×259 for LiCl. The number of reciprocal lattice vectors is 387 for diamond and 331 for LiCl. The plasmon-pole model of von der Linden and Horsch (Ref. 9) is used. Here E_g is the indirect band gap of diamond, all the other minimum band gaps are underlined. Our results are compared with the LAPW, PP, and experimental results.

	LDA		GWA		Expt. [b]
	Present	PP [a]	Present	PP [a]	
Diamond					
$\Gamma'_{25v}\rightarrow\Gamma_{1c}$	5.53	5.58	7.39 (7.41)	7.5; 7.63 [c]	7.3
$\Gamma'_{25v}\rightarrow X_{1c}$	4.61	4.63	6.19 (6.27)	6.30 [c]	
$\Gamma'_{25v}\rightarrow L_{1c}$	8.38	8.39	10.36 (10.38)	10.23 [c]	
E_g	4.01	4.01	5.60	5.6; 5.67 [c]	5.48
LiCl					
$\Gamma'_{15v}\rightarrow\Gamma_{1c}$	5.86	6.0	8.75(8.66)	9.1	9.4 [d]
$\Gamma'_{15v}\rightarrow X_{1c}$	7.54	7.5	10.50 (10.45)	10.7	
$\Gamma'_{15v}\rightarrow L_{1c}$	6.50	6.4	9.36 (9.32)	9.7	

[a]Unless noted, Ref. 3.
[b]Unless noted, Ref. 44.
[c]Reference 60.
[d]Reference 63.

Figure 4 shows the LDA and GWA calculated minimum band gaps for all studied semiconductors, and are compared with the corresponding PP and experimental results. A perfect agreement with experiment is achieved when the calculated value falls on the dashed line. We notice that for most of the small- and medium-band-gap semiconductors GWA does not account for the whole correction of the band gap. The disagreement with the experiment is most probably due to the neglect of the core-polarization interaction,[16] and to effects beyond the GWA.[10] In fact, it is interesting to mention that a first-order vertex and self-consistent corrections to the RPA polarizability and to the self-energy within the GWA increase the direct energy band gaps of Si at the Γ, L, and X points by about 0.36, 0.44, and 0.39 eV, respectively.[10] These corrections seem to be large but are indicative of an upwards correction. If this is true then it seems then that there is no compensation between the vertex correction and the self-consistency as for the jellium model. An improvement for these calculations is to start from the self-consistent Green's function as suggested by Hedin[1] instead of the noninteracting Green's function. At the present time it looks like the question of the band gaps of small- and medium-band-gap semiconductors is not fully solved.

B. Quasiparticle results of wide-band-gap semiconductors and insulators: Diamond and LiCl

It is of interest to compare our all-electron GWA calculations for wide-band-gap semiconductors and insulators with existing PP calculations. Wide-band-gap semiconductors are somehow puzzling in contrast to small- and medium-band-gap semiconductors: While the LDA band gaps of these materials are significantly underestimated compared with ex-

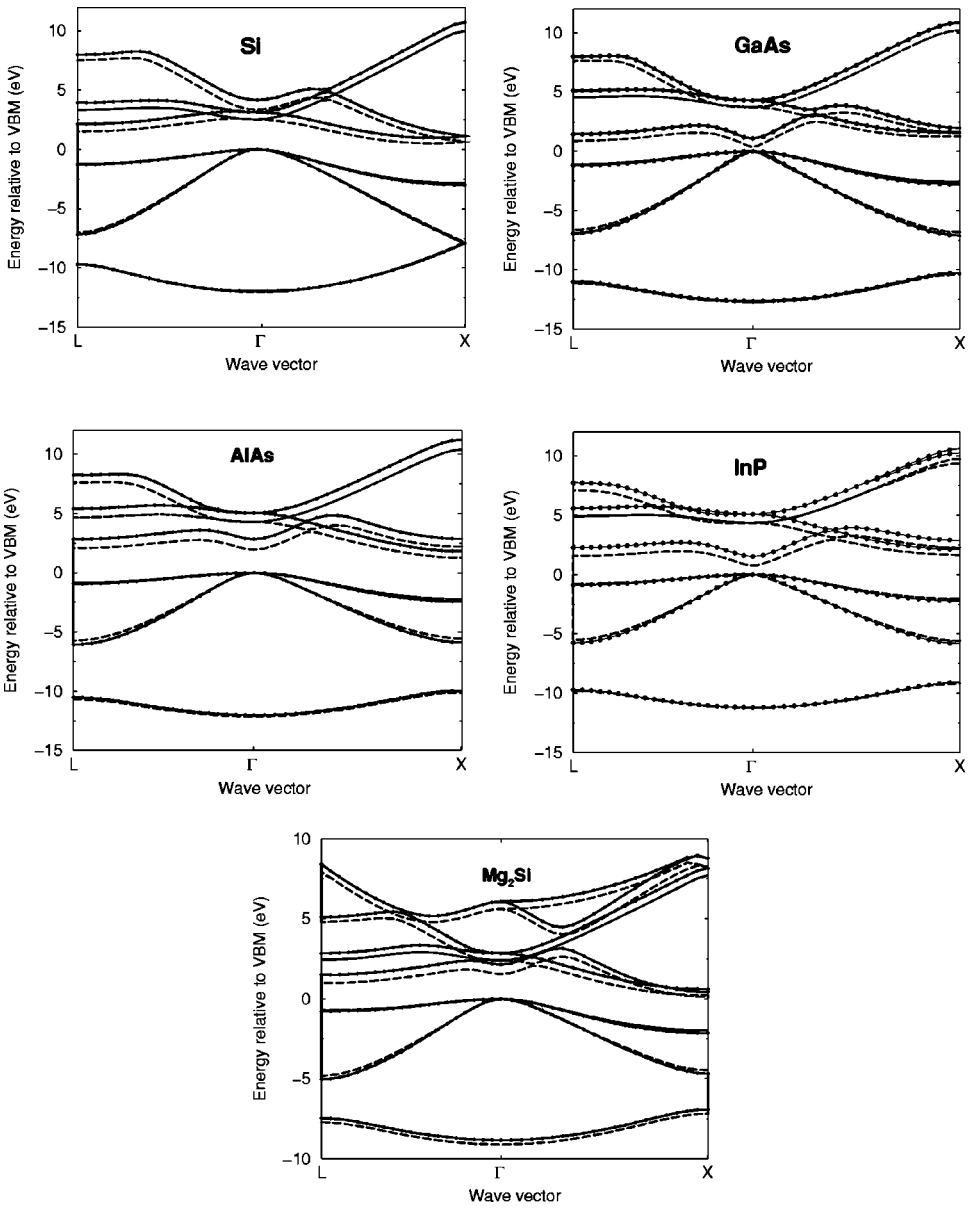

FIG. 3. Calculated electronic band structures along high-symmetry directions for some small- and medium-band-gap semiconductors: Si, GaAs, AlAs, InP, and $SiMg_2$ (in eV). The dashed lines display the LDA results calculated with an energy cutoff of 15 Ry (cf. Tables V and VI, column 2). The solid lines with dots show the GWA results based on these LDA results (cf. Tables V and VI, column 3). The energy scale is relative to the top of the valence-band maximum (VBM).

periment, the LDA static dielectric functions are usually in good agreement with the experimental results, see for example Refs. 56 and 58.

Table VII shows the calculated PAW-LDA and PAW-GWA band energies for the high-symmetry points Γ, X, and L for wide-band-gap semiconductors: diamond and LiCl, respectively. These results are compared with other PP-GWA calculations[3,60] and with experimental data whenever available.[44,61–63] Figure 5 presents the corresponding band structures along the $L\Gamma$ and ΓX high-symmetry directions.[64] For diamond the calculated QP eigenvalues are in good agreement with experiment and PP calculations. For LiCl only the experimental band gap is available and is slightly larger than our GWA value. It is worth mentioning that we did not update the Green's function to get our GWA values as in the PP calculation of Hybertsen and Louie.[3] Such a procedure increases the GWA band gap by about 0.3 eV and leads to a better agreement with PP results of Hybertsen and Louie.[3] For these wide-band-gap materials we investigated also the applicability of the scissors-operator shift and found that it is accurate only to within 0.32 and 0.28 eV for dia-

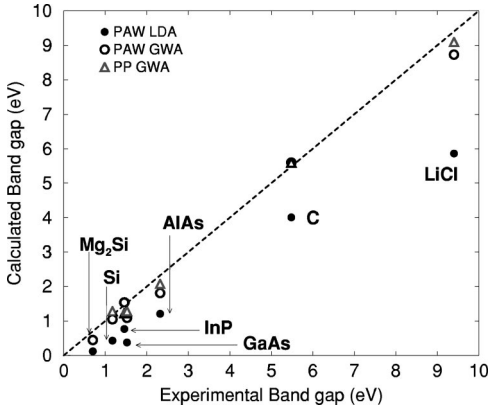

FIG. 4. Calculated LDA and GWA energy band gaps compared with experimental and PP-GWA results of Ref. 16. The filled circles represent the LDA values, the open circles the PAW-GWA values, and the up-triangles the PP GWA. A perfect agreement with experiment is achieved when a calculated value is on the dashed line.

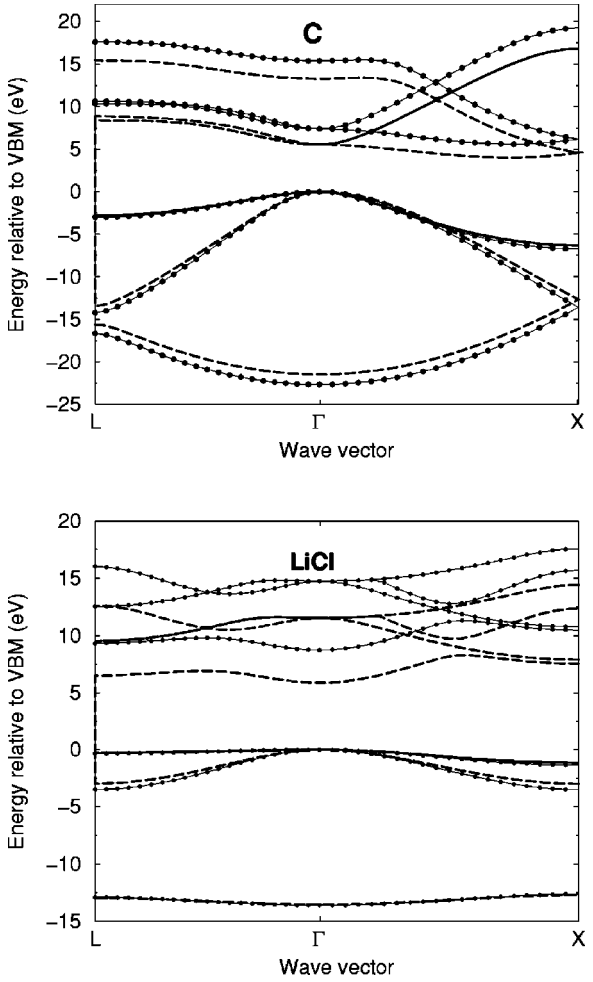

FIG. 5. Calculated electronic band structures along ΓX and ΓL high-symmetry lines of some wide-band-gap semiconductors: diamond and LiCl (in eV). The dashed lines display the LDA results calculated with an energy cutoff of 45 Ry for diamond and 20 Ry for LiCl (cf. Table VII, column 2). The solid lines with dots show the GWA results based on these LDA results (cf. Tables VII, column 3). The energy scale is relative to the top of the valence-band maximum (VBM).

mond and LiCl, respectively. These energy deviations are somewhat larger in absolute values (about twice the value found for GaAs) than for small- and medium-band-gap semiconductors. These large energy deviations question the use of the scissors-operator shift for the computation of optical properties. However, if we compare these energy deviations with the size of the band gap, the largest ratio occurs for diamond and is only 5% compared to the 10% ratio for a medium-band-gap semiconductor such as GaAs.

IV. CONCLUSION

We have implemented an all-electron GWA using the recently developed projector-augmented-wave method.[31] The knowledge of the one-electron Green's function of the PAW Hamiltonian allows us to construct the QP self-energy within the GWA, in which the dynamical screening of the electron-electron interaction arises from a plasmon-pole model dielectric function[9,12,32] for which the parameters are adjusted to the dielectric function calculated using the RPA. We have tried various plasmon-pole model dielectric functions for the screening of the Coulomb interaction and showed that the QP energies are not sensitive to the type of the model used.

Using this GWA method, we have determined the GWA QP electronic structure of Mg_2Si. Our LDA results are in good agreement with the empirical pseudopotential, and the GWA shifts almost rigidly the empty states by about 0.32 eV towards higher energies.

Concerning the other semiconductors studied here, we have found an overall agreement of our calculated electronic structure of various semiconductors with existing GWA pseudopotential calculations performed by different groups,[3,7,13,16,41,42,60] and with experimental results.[44–55,61–63] Nevertheless, for a detailed comparison, most of the all-electron GWA small- and medium-band-gap semiconductors are slightly smaller that the PP results and most of this difference is attributed to the discrepancy in the exchange-correlation matrix elements. On the other-hand, the first order vertex and self-consistent corrections to the RPA polarizability and to the self-energy within the GWA are shown to increase the direct energy band gaps of Si at the Γ, L, and X points by a few tenths of an electron volt,[10] showing that there is some room for an upward correction.

To our knowledge this is the first full-potential all-electron GWA calculation that has corrected the LDA eigenvalues for three type of semiconductors, small- medium-, and wide-band-gap semiconductors, and that has questioned the accuracy of the energy band gaps of semiconductors obtained by means of the PP-GWA *without* core-polarization interaction.

ACKNOWLEDGMENTS

We would like to thank P. Blöchl for providing us with his PAW code and for useful discussions. Part of this work was done during our visit to the Ohio State University, and we would like to thank J. W. Wilkins and W. Aulbur for useful discussions. We would also like to thank E. Shirley and V. Olevano for providing us with the details of their LDA and *GW* PP results. The supercomputer time was granted by CINES on the IBM SP2 supercomputer (Project No. gem1100). IPCMS is a UMR CNRS-ULP 7504.

APPENDIX: USE OF SYMMETRY TO REDUCE THE COMPUTATIONAL COST OF THE GWA

The transformation of a Bloch wave function $\Psi_{\mathbf{k}n}$ under a symmetry operation R of a symmorphic point group is given by

$$\Psi_{\mathbf{k}n}(R^{-1}\mathbf{r}) = \sum_m D(R)_{nm}\Psi_{R\mathbf{k}m}(\mathbf{r}), \qquad \text{(A1)}$$

where $D(R)_{nm}$ denote the unitary transformation associated with the symmetry operation R. If the state $\Psi_{\mathbf{k}n}$ is nondegenerate, the transformation rule of the wave function simplifies greatly since $D(R)_{nm} = \delta_{nm}$. We suppose now that the states considered here are nondegenerate to simplify the discussion. Using such a relation it can be shown that the matrix elements defined by Eq. (17) satisfy the following relation:

$$M_{\mathbf{G}}^{nm}(\mathbf{k},R\mathbf{q})=M_{R^{-1}\mathbf{G}}^{nm}(\mathbf{k},\mathbf{q}) \quad \text{for } R\mathbf{k}=\mathbf{k}. \tag{A2}$$

This relation is valid for all the symmetry operations belonging to the little group $G_{\mathbf{k}}$ of the point group G. Then, it can be shown that the integrand appearing in the Hartree-Fock contribution defined by Eq. (13) is invariant under the symmetry operations belonging to $G_{\mathbf{k}}$. Such a symmetry property reduces the number of $\mathbf{q}$ points for which the integrand has to be calculated. Indeed, if $B_{\mathbf{k}}$ denotes the irreducible BZ defined by the elements of $G_{\mathbf{k}}$, the Hartree-Fock contribution can be rewritten as

$$\langle\Psi_{\mathbf{k}n}|\Sigma^{HF}|\Psi_{\mathbf{k}n}\rangle=-\frac{4\pi}{\Omega}\sum_{\mathbf{q}\in B_{\mathbf{k}}}w(\mathbf{q})\sum_{m\ occ}\sum_{\mathbf{G}}\frac{|M_{\mathbf{G}}^{mn}(\mathbf{k},\mathbf{q})|^2}{|\mathbf{q}+\mathbf{G}|^2} \tag{A3}$$

where $w(\mathbf{q})$ denotes the weight of the $\mathbf{q}$ point. In the case where the state $\Psi_{\mathbf{k}n}$ happens to be degenerate, we should sum the matrix elements over all degenerate states to get an invariant integrand. The same type of symmetry reduction holds for the calculation of the symmetrized static dielectric matrix using the fact that $\epsilon_n(R\mathbf{k})=\epsilon_n(\mathbf{k})$ and

$$M_{\mathbf{G}}^{nm}(R\mathbf{k},\mathbf{q})=M_{R^{-1}\mathbf{G}}^{nm}(\mathbf{k},\mathbf{q}) \quad \text{for } R\mathbf{q}=\mathbf{q}. \tag{A4}$$

We obtain

$$\tilde{\epsilon}_{\mathbf{G}\mathbf{G}'}(\mathbf{q},\omega=0)=\delta_{\mathbf{G}\mathbf{G}'}-\frac{16\pi}{\Omega|\mathbf{q}+\mathbf{G}||\mathbf{q}+\mathbf{G}'|}\times\sum_{\mathbf{k}\in B_{\mathbf{q}}}\sum_{v,c}\sum_{R\in G_{\mathbf{q}}}\frac{M_{R\mathbf{G}}^{vc}(\mathbf{k},\mathbf{q})[M_{R\mathbf{G}'}^{vc}(\mathbf{k},\mathbf{q})]^*}{\epsilon_v(\mathbf{k}-\mathbf{q})-\epsilon_c(\mathbf{k})}. \tag{A5}$$

The relationship between the matrix elements of $\tilde{\epsilon}_{\mathbf{G}\mathbf{G}'}$ also reduces the computational cost. Using the symmetry property of the symmetrized dielectric function $\tilde{\epsilon}(\mathbf{r},\mathbf{r}')=\tilde{\epsilon}(R\mathbf{r},R\mathbf{r}')$, it can be shown that

$$\tilde{\epsilon}_{\mathbf{G}\mathbf{G}'}(R\mathbf{q},\omega=0)=\tilde{\epsilon}_{R^{-1}\mathbf{G}R^{-1}\mathbf{G}'}(\mathbf{q},\omega=0). \tag{A6}$$

So both the Hermiticity of $\tilde{\epsilon}$ and the relationship between the matrix elements which results from the symmetry operations leaving $\mathbf{q}$ invariant are used to reduce the number of matrix elements to be computed. Now, we have to remember that the plasmon-pole parameters in the von der Linden–Horsch model are obtained by solving an eigenvalue problem

$$\int d\mathbf{r}'\ \tilde{\epsilon}(\mathbf{r},\mathbf{r}')\phi^p(\mathbf{q},\mathbf{r}')=\lambda_p(\mathbf{q})\phi^p(\mathbf{q},\mathbf{r}). \tag{A7}$$

By analogy with the resolution of the Schrödinger-type equation in a crystal, it can be shown that

$$\phi_{\mathbf{G}}^p(R\mathbf{q})=\phi_{R^{-1}\mathbf{G}}^p(\mathbf{q}) \quad \text{and} \quad \lambda_p(R\mathbf{q})=\lambda_p(\mathbf{q}). \tag{A8}$$

These symmetry properties can be used to show the invariance of the force and the frequency of the pole,

$$z_p(R\mathbf{q})=z_p(\mathbf{q}) \quad \text{and} \quad \omega_p(R\mathbf{q})=\omega_p(\mathbf{q}). \tag{A9}$$

If the point group G of the crystal does not contain the inversion symmetry, the time-reversal symmetry could be implemented. Because of these symmetry relations, the eigenvectors and eigenvalues of the symmetrized dielectric matrix are only computed for irreducible $\mathbf{q}$ points with respect to the point group of the crystal. Now it can be shown that the integrand appearing in the contribution to the self-energy given by Eq. (14) is invariant under symmetry operations belonging to the little group of $\mathbf{k}$ denoted $G_{\mathbf{k}}$ as in the case of the Hartree-Fock contribution.

[1] L. Hedin, Phys. Rev. **139**, A796 (1965).
[2] L. Hedin and S. Lundquist, in *Solid State Physics*, edited by H. Ehrenreich, F. Seitz, and D. Turnbull (Academic, New York, 1969), Vol. 23, p. 1.
[3] M.S. Hybertsen and S.G. Louie, Phys. Rev. B **34**, 5390 (1986); Comments Condens. Matter Phys. **13**, 223 (1987).
[4] M.S. Hybertsen and S.G. Louie, Phys. Rev. B **35**, 5585 (1987).
[5] R.W. Godby, M. Schlüter, and L.J. Sham, Phys. Rev. B **37**, 10 159 (1988).
[6] R.W. Godby, M. Schlüter, and L.J. Sham, Phys. Rev. B **35**, 4170 (1987).
[7] R.W. Godby and R.J. Needs, Phys. Rev. Lett. **62**, 1169 (1989).
[8] W. von der Linden, P. Fulde, and K.-P. Bohnen, Phys. Rev. B **34**, 1063 (1986).
[9] W. von der Linden and P. Horsch, Phys. Rev. B **37**, 8351 (1988).
[10] R.T. Ummels, P.A. Bobbert, and W. van Haeringen, Phys. Rev. B **57**, 11 962 (1998).
[11] P.A. Bobbert and W. van Haeringen, Phys. Rev. B **49**, 10 326 (1994).
[12] N. Hamada, M. Hwang, and A.J. Freeman, Phys. Rev. B **41**, 3620 (1990).
[13] R. Hott, Phys. Rev. B **44**, 1057 (1991).
[14] F. Aryasetiawan, Phys. Rev. B **46**, 13051 (1992).
[15] E.L. Shirley and S.G. Louie, Phys. Rev. Lett. **71**, 133 (1993).
[16] E.L. Shirley, X. Zhu, and S.G. Louie, Phys. Rev. Lett. **69**, 2955 (1992); Phys. Rev. B **56**, 6648 (1997).
[17] F. Araysetianwan and O. Gunnarsson, Rep. Prog. Phys. **61**, 237 (1998).
[18] W.G. Aulbur, L. Jönsson, and J. W. Wilkins, in *Solid State Physics*, edited by H. Ehrenreich (Academic, Orlando, 1999), Vol. 54, p. 1.
[19] L. Hedin, J. Phys.: Condens. Matter **11**, R489 (1999).
[20] J.E. Northrup, M.S. Hybertsen, and S.G. Louie, Phys. Rev. B **39**, 8198 (1989).
[21] S. Saito, S.B. Zhang, S.G. Louie, and M.L. Cohen, Phys. Rev. B **40**, 3643 (1989).
[22] X. Zhu and S.G. Louie, Phys. Rev. B **43**, 12 146 (1991).
[23] J.E. Northrup and S.B. Zhang, Phys. Rev. B **47**, l0 032 (1993).
[24] S.B. Zhang, M.L. Cohen, S.G. Louie, D. Tománek, and M.S. Hybertsen, Phys. Rev. B **41**, 10 058 (1990).
[25] S.B. Zhang, M.S. Hybertsen, M.L. Cohen, S.G. Louie, and D. Tománek, Phys. Rev. Lett. **63**, 1495 (1989).
[26] E.L. Shirley and R.M. Martin, Phys. Rev. B **47**, 15 404 (1993).
[27] J.P.A. Charlesworth, R.W. Godby, R.J. Needs, and L.J. Sham, Mater. Sci. Eng., B **14**, 262 (1992).
[28] S. Albrecht, L. Reining, R. Del Sole, and G. Onida, Phys. Rev. Lett. **80**, 4510 (1998).

[29] L.X. Benedict, E.L. Shirley, and R.B. Bohn, Phys. Rev. Lett. **80**, 4514 (1998); Phys. Rev. B **57**, R9385 (1998).
[30] M. Rohlfing and S.G. Louie, Phys. Rev. Lett. **81**, 2312 (1998).
[31] P.E. Blöchl, Phys. Rev. B **50**, 17 953 (1994).
[32] G.E. Engel and B. Farid, Phys. Rev. B **47**, 15 931 (1993).
[33] S.L. Adler, Phys. Rev. **126**, 413 (1962); N. Wiser, *ibid.* **129**, 62 (1963).
[34] P. Hohenberg, and W. Kohn, Phys. Rev. **136**, 864 (1964); W. Kohn and L.J. Sham, *ibid.* **140**, A1113 (1965).
[35] W. G. Aulbur, Ph.D. thesis, The Ohio State University, 1996.
[36] H. Raether, *Excitation of Plasmons and Interband Transitions by Electrons*, Springer Tracts in Modern Physics Vol. 88 (Springer, New York, 1980).
[37] H.J. Monkhorst and J.D. Pack, Phys. Rev. B **13**, 5188 (1976).
[38] F. Gygi and A. Baldereschi, Phys. Rev. B **34**, 4405 (1986).
[39] S.G. Louie, S. Froyen, and M.L. Cohen, Phys. Rev. B **26**, 1738 (1982).
[40] S. Massida, M. Posternak, and A. Baldereschi, Phys. Rev. B **48**, 5058 (1993).
[41] V. Olevano (private communication). The calculations are performed using the *GW* numerical code developed by A. Godby and co-workers (see Ref. 7).
[42] E. Shirley (private communication). Shirley suggested that the differences between his calculated Σ^{HF} and Σ and that of Olevano is most probably due to the use of different pseudopotential setups and different types of plasmon-pole models.
[43] We have found for small- and medium-band-gap semiconductors that our results using two Chadi-Cohen **k** points [see J. Chadi and M.L. Cohen, Phys. Rev. B **8**, 5747 (1973)] corresponding to 32 **k** points in the whole BZ and the most converged values using ten special **k** points (Ref. 37) (256 **k** points in the BZ) differ by as much as 0.2 eV. It is worth mentioning that most of the data in the literature are produced using about 32 **k** points in the BZ and are therefore *not* converged.
[44] *Numerical Data and Functional Relationships in Science and Technology*, edited by K.H. Hellwege and O. Madelung, Landolt-Börnstein, New Series, Group III, Vols. 17 and 22, Part a (Springer, Berlin, 1982).
[45] J.E. Ortega and F.J. Himpsel, Phys. Rev. B **47**, 2130 (1993).
[46] W.E. Spicer and R. C. Eden, in *Proceedings of the Ninth International Conference on the Physics of Semiconductors, Moscow, 1968*, edited by S. M. Ryvkin (Nauka, Leningrad, 1968), Vol. 1, p. 61.
[47] A.L. Wachs, T. Miller, T.C. Hsieh, A.P. Shapiro, and T.C. Chiang, Phys. Rev. B **32**, 2326 (1985).
[48] F.J. Himpsel, P. Heimann, and D.E. Eastman, Phys. Rev. B **24**, 2003 (1981).
[49] R. Hulthen and N.G. Nilsson, Solid State Commun. **18**, 1341 (1976).
[50] D. Straub, L. Ley, and F.J. Himpsel, Phys. Rev. Lett. **54**, 142 (1985).
[51] D.J. Wolford and J.A. Bradley, Solid State Commun. **53**, 1069 (1985).
[52] D.E. Aspnes and A.A. Studna, Phys. Rev. B **27**, 985 (1983); D.E. Aspnes, S.M. Kelso, R.A. Logan, and R. Bhatt, J. Appl. Phys. **60**, 754 (1986).
[53] M. Cardona, N.E. Christensen, and G. Fasol, Phys. Rev. B **38**, 1806 (1988).
[54] P. Lautenschlager, M. Garriga, S. Logothetidis, and M. Cardona, Phys. Rev. B **35**, 9174 (1987).
[55] M.W. Heller and G.C. Damielson, J. Phys. Chem. Solids **23**, 601 (1962).
[56] J. Chen, Z.H. Levine, and J.W. Wilkins, Appl. Phys. Lett. **66**, 1129 (1995).
[57] Z.H. Levine and D.C. Allan, Phys. Rev. B **43**, 4187 (1991).
[58] M. Alouani and J. M. Wills, *Electronic Structure and Physical Properties of Solids*, edited by H. Dreysse (Springer, New York, 1998), p. 168; Phys. Rev. B **54**, 2480 (1996).
[59] M.Y. Yang and M.L. Cohen, Phys. Rev. **178**, 1358 (1969); Solid State Commun. **6**, 855 (1968).
[60] M. Rohlfing, Peter Krüger, and J. Pollmann, Phys. Rev. B **48**, 17 791 (1993).
[61] F.R. McFeely *et al.*, Phys. Rev. B **9**, 5268 (1974).
[62] F.J. Himpsel, J.F. van der Veen, and D.E. Eastman, Phys. Rev. B **22**, 1967 (1980).
[63] G. Baldini and B. Bosacchi, Phys. Status Solidi **38**, 325 (1970).
[64] The diamond and LiCl QP energies computed using 32**k** points and 256**k** points in the BZ are in good agreement.